ACS APPLIED MATERIALS & INTERFACES

Research Article

www.acsami.org

Local Ion Irradiation-Induced Resistive Threshold and Memory Switching in Nb_2O_5/NbO_x Films

Helge Wylezich,*[,†] Hannes Mähne,[†] Jura Rensberg,[‡] Carsten Ronning,[‡] Peter Zahn,[§] Stefan Slesazeck,*[,†] and Thomas Mikolajick[†,∥]

[†]NaMLab gGmbH, Nöthnitzer Str. 64, D-01187 Dresden, Germany

[‡]Institute for Solid State Physics, University of Jena, Helmholtzweg 3, D-07743 Jena, Germany

[§]Helmholtz−Zentrum Dresden−Rossendorf, Bautzner Landstr. 400, D-01328 Dresden, Germany

[∥]Chair of Nanoelectronic Materials, Institute of Semiconductor and Microsystems, Faculty of Electrical and Computer Engineering, TU Dresden, Nöthnitzer Str. 64, D-01187 Dresden, Germany

Supporting Information

ABSTRACT: Resistive switching devices with a Nb_2O_5/NbO_x bilayer stack combine threshold and memory switching. Here we present a new fabrication method to form such devices. Amorphous Nb_2O_5 layers were treated by a krypton irradiation. Two effects are found to turn the oxide partly into a metallic NbO_x layer: preferential sputtering and interface mixing. Both effects take place at different locations in the material stack of the device; preferential sputtering affects the surface, while interface mixing appears at the bottom electrode. To separate both effects, devices were irradiated at different energies (4, 10, and 35 keV). Structural changes caused by ion irradiation are studied in detail. After successful electroforming, the devices exhibit the desired threshold switching. In addition, the choice of the current compliance defines whether a memory effect adds to the device. Findings from electrical characterization disclose a model of the layer modification during irradiation.

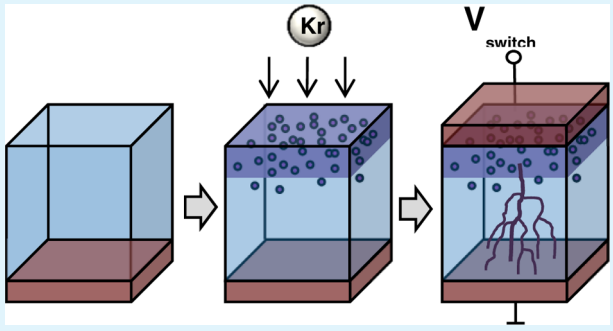

KEYWORDS: *resistive switching, threshold switching, niobium oxide, ion irradiation*

INTRODUCTION

In the last years research on semiconductor memories brought resistive memories into focus as one of the most promising candidates for next-generation nonvolatile memories because of the excellent scalability of these memories.[1−3] However, one issue to be solved is the sneak-path problem in cost efficient cross-bar arrays. In cross-point memory arrays, neighboring cells interfere with each other making it difficult to operate the array.[4] By using metal−insulator−semiconductor (MIS) transistors as a switch the problem could be solved, but at the expense of limiting the memory layers to one per chip.[5] A better choice is to integrate a bidirectional switch directly into the memory element. This approach saves fabrication cost by stacking more than one memory layer directly above CMOS logic. A possible approach is to integrate a threshold switch together with the memory switch. An example for a material that enables such a configuration is niobium oxide. In the stoichiometric case Nb_2O_5 shows memory switching, while in the oxygen-deficient NbO_2 configuration it exhibits threshold switching.[6,7] By stacking the two layers accordingly the resulting structure combines the memory device with a selection element.[8−11] Several methods are reported to fabricate such a device: one possibility is to deposit a thin niobium film and to use different oxidation conditions.[11] Nevertheless, the disadvantage of this process is the necessity of a high-temperature treatment. Furthermore, niobium oxide films can be sputtered, either by magnetron sputtering from a Nb_2O_5 target[10] or reactively from a niobium target.[8] In the latter case the deposition is done at room temperature, which minimizes the thermal budget of the process. However, the Nb_2O_5/NbO_2 stack must be structured after fabrication; otherwise, the low-resistive NbO_2 layer will short adjacent electrodes and make the operation of arrays impossible.

In this paper, we report a new method to fabricate a Nb_2O_5/NbO_x stack. Nb_2O_5 was reactively sputtered and afterward treated by krypton ion irradiation. Ion irradiation and implantation is a well-established industrial technique for both structuring and/or doping of materials. Here, we used noble gas atoms as they are neither incorporated into the niobium oxide lattice nor actively affect any electrical properties and are therefore the ideal species to study the effects caused by ion irradiation.

The energy of each incident ion is transferred to the target by numerous inelastic collisions with the target atoms, known as

Received: April 7, 2014
Accepted: September 12, 2014
Published: September 12, 2014

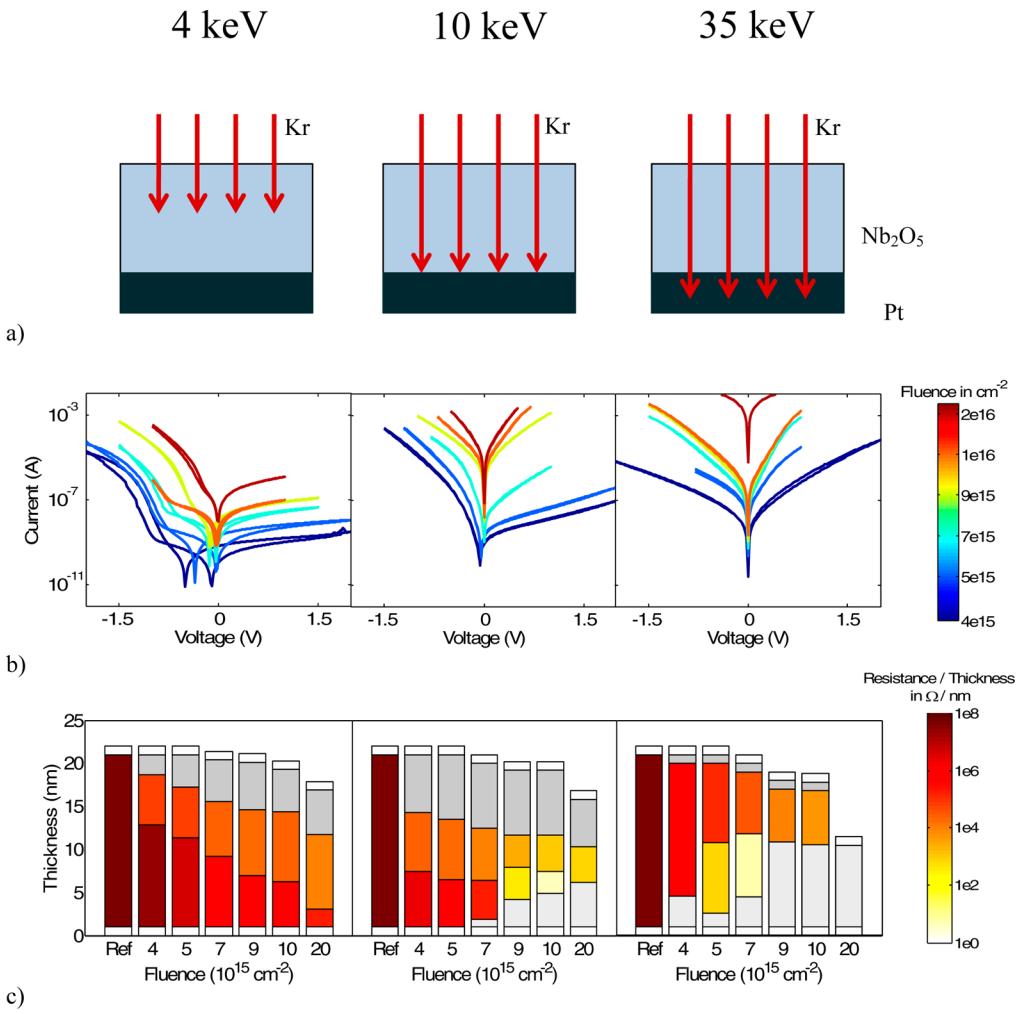

Figure 1. Effects of the krypton irradiation. (a) Irradiation energy was chosen to affect different regions of the sample: the upper part of the oxide (left column), the complete oxide (middle column), the complete oxide and the bottom electrode (right column). (b) $I-V$ characteristics of devices irradiated with krypton ions at different ion energies and fluences ranging from 4×10^{15} cm^{-2} to 2×10^{16} cm^{-2} as defined by the color bar. (c) Model of the devices after krypton irradiation. The bottom and top electrodes are white, the metallic NbO_x layer dark gray at the top and light gray at the bottom electrode. The color of the insulating Nb_2O_5 layer displays the small signal resistance per nm according to the color scale of the bar. Generally, a lighter color means a lower resistivity in the model.

collision cascade. As a result of this ion−solid interaction three different processes can transform the oxide layer Nb_2O_5 into a metallic NbO_x layer. First, surface atoms are removed if they receive sufficient energy to overcome the surface binding energy, which is the so-called "sputtering" process. In addition to layer thinning, oxygen can be preferentially sputtered, because of the lower surface binding energy of oxygen atoms compared to niobium atoms resulting in an oxygen-deficient and niobium-rich metallic surface layer.[12,13] Second, if the ion energy is high enough, the collision cascade ranges into the bottom electrode, and a fraction of the atoms of the bottom electrode are backscattered into the oxide layer. Thus, interface mixing can cause a metallic interface layer at the bottom electrode. Third, above a certain energy threshold the energy transfer from ions to lattice atoms cause bond breaking and therefore a displacement of the Nb and O atoms from their lattice sides. Although the oxide bond (Nb−O) of Nb_2O_5 is energetically favored, metallic bonds (Nb═O) can be formed during this process. Hence, krypton irradiation offers the possibility to form a device stack with a metallic layer either at the top or at the bottom electrode, which is known to combine threshold and memory switching. Integrated into a dense crossbar array, the metallic layer would short adjacent electrodes. However, by adopting an irradiation mask, the formation of the metallic layer can be restricted to the point of intersection of top and bottom electrodes. This approach lacks the need of further structuring the Nb_2O_5/NbO_x stack and hence offers a further degree of freedom during manufacturing.

RESULTS AND DISCUSSION

Impact of the Ion Irraditation. The investigated devices consist of 20 nm of amorphous Nb_2O_5 sandwiched between two platinum electrodes. The bottom electrode is unstructured, while the top electrodes are defined by a shadow mask with a pitch of 100 μm to prevent crosstalk in electrical measurements. Three sample series were irradiated with different krypton ion energies, thus attaining different penetration depths (Figure 1a). The irradiation was performed before the Pt top electrode deposition. The first series was irradiated with 4 keV Kr ions, which leads to a projected ion range with a straggle of $R_p = (4.7 \pm 2.0)$ nm, and a maximum penetration depth of $R_{max} \approx 10$ nm as simulated using the TRIM code.[14] By increasing the

dx.doi.org/10.1021/am5021149 | ACS Appl. Mater. Interfaces 2014, 6, 17474−17480

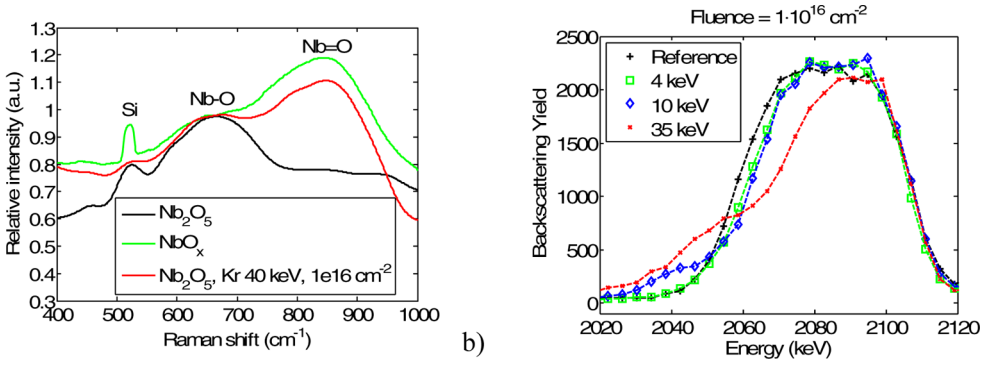

Figure 2. (a) Raman spectrum of niobium oxide reactively sputtered in oxide mode (Nb_2O_5), in metallic mode (NbO_x), and irradiated with krypton ions at an energy of 40 keV and a fluence of 1×10^{16} cm^{-2}. All curves are normalized to the same peak height at 670 cm^{-1}. In contrast to the other devices, the oxide thickness is 50 nm to improve measurement resolution. (b) Niobium peak of the RBS spectrum for a pristine device and devices irradiated with 4, 10, and 35 keV krypton ions at an ion fluence of 1×10^{16} cm^{-2} with an initial oxide thickness of 20 nm.

irradiation energy to 10 keV, ions are ranging deeper; nevertheless, all ions are stopped before reaching the bottom electrode [R_P = (8.0 ± 3.4) nm, $R_{max} \approx$ 20 nm]. Hence, the complete oxide layer is affected. Increasing the ion energy further to 35 keV, the ions are stopped at the oxide layer/bottom electrode interface [R_P = (16.8 ± 6.2) nm, $R_{max} \approx$ 30 nm]. Therefore, interface mixing must be taken into account only for this situation. Each sample series was irradiated with different ion fluences, ranging from 4×10^{15} cm^{-2} to 2×10^{16} cm^{-2}. In addition an untreated pristine device was investigated as reference.

At first, we investigated the material changes caused by the krypton irradiation. Figure 2a displays the Raman spectrum of niobium oxide samples prepared at different oxygen partial pressures and of an irradiated sample. By decreasing the oxygen partial pressure during growth the niobium exhibits lower oxidation states ($Nb_2O_5 \rightarrow NbO_x$). While Nb_2O_5 shows a significant peak at 670 cm^{-1}, with decreasing oxygen partial pressure a second peak arises at around 850 cm^{-1}. The first peak is attributed to oxidic bonds (Nb−O), and the second is attributed to metallic bonds (Nb═O).[15,16] After ion treatment the same characteristic peak appears at 850 cm^{-1}, indicating the formation of a metallic NbO_x layer. Although the Raman spectrum clearly confirms the existence of metallic bonds after ion irradiation, it does not give information about the position of those bonds within the switching layer.

Current−voltage (I−V) characteristics were taken and are shown in Figure 1b. For all electrical measurements the bias was applied to the top electrode, while the bottom electrode was grounded. The step voltage of the I−V characteristic was V_{step} = 20 mV. In the virgin state (Supporting Information, Figure S1) the difference in work function of Pt (W = 5.65 eV)[17] and electron affinity of Nb_2O_5 (E_A = 4.0 eV)[18] forms two opposite Schottky barriers at the bottom and top electrode, which prevent a significant current flow. Irradiating the sample with 4 keV krypton ions results in a considerable unsymmetric I−V characteristic (Figure 1b, left). In this case, charge carriers can pass the barrier at the top electrode, while the Schottky barrier at the bottom electrode remains unaltered. This characteristic can be explained by both an increased defect density of the oxide near the top electrode as well as the formation of a substochiometric NbO_x interface layer, which converts the Schottky barrier into an ohmic contact. Although for the 4 keV irradiation the unsymmetric behavior is independent of the ion fluence, the current level increases with increasing ion fluence due to the thinning of the oxide layer and due to the increased irradiation defects along the layer caused by collision cascades. A different dependence is obtained for the 10 keV series. For low ion fluences the I−V characteristic is also strongly asymmetrical, but an overall higher current level flows through the devices. For increasing ion fluences beyond 5×10^{15} cm^{-2} the device becomes nearly symmetrical, indicating a slightly lower barrier at the bottom electrode. The sputtering becomes significant in such a case (see below) and decreases the film thickness, so the interface to the bottom electrode is also being irradiated. At an energy of 35 keV the I−V characteristic is reversed. Even for low fluences the current level for positive voltage polarity is higher than it is for negative voltage polarity. It appears that the defect density of the NbO_x layer near the bottom electrode is now higher compared to the interface at the top electrode. Increasing the ion fluence to 2×10^{16} cm^{-2} yields an ohmic characteristic with a resistance of R = 41 Ω. Under these conditions the remaining part of the originally insulating Nb_2O_5 layer becomes completely metallic.

Furthermore, Rutherford backscattering spectrometry (RBS) gives information about the origin of the metallic layer. By means of RBS no remaining krypton was found in any of the investigated samples, indicating that the krypton has diffused out. Hence, the metallic layer is originated by structural defects caused by the krypton irradiation, not by the ions itself. For all ion energies and a fixed ion fluence of 1×10^{16} cm^{-2} Figure 2b shows the niobium part of the respective RBS spectrum attributed to the niobium oxide layer (full RBS spectra are depicted in Supporting Information, Figure S2). The left edge of the peak displays the interface to the platinum bottom electrode, and the right edge displays the surface of the oxide since the measurements were done before top electrode deposition. It can be seen that in comparison to a pristine reference sample the width of the niobium peak is decreased, and the overall form is changed for the irradiated samples. On the one hand, this decrease in width can be attributed to surface sputtering reducing the oxide layer thickness. On the other hand, for ion energies starting at 10 keV a significant niobium backscattering yield is found at lower RBS energies, which could be caused by either a rougher oxide surface or by the mixing of the niobium oxide and the platinum bottom electrode. The depths of the backscattering signal points to interface mixing, and from atomic force microscope measurements we could exclude that the surface roughness increases by

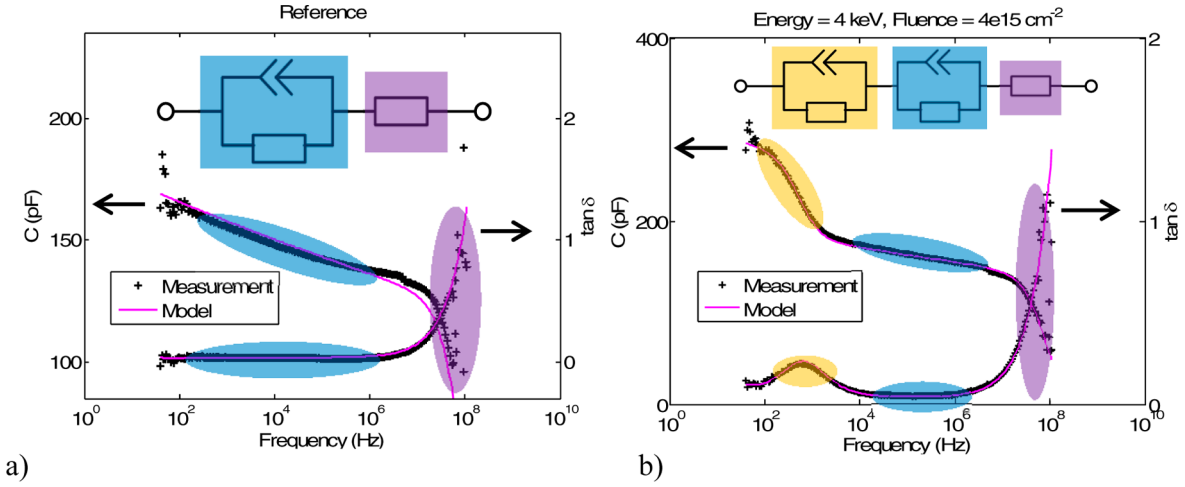

Figure 3. Complex impedance in dependence of frequency. (a) Reference device and (b) a device irradiated with krypton ions at an energy of 4 keV and a fluence of 4×10^{15} cm^{-2}. The insertion shows the equivalent circuit used for fitting the measured data. The colors mark the part of the equivalent circuit that is dominating the behavior in the frequency range marked by the same color as the respective circuit element.

the ion treatment (see Supporting Information, Figure S3 for more details). Independent of the Kr ion energy, a significant layer thickness reduction is observed starting at a fluence of 9×10^{15} cm^{-2}. The total thickness reduction was determined quantitatively by fitting the RBS spectrum using the ion beam analysis code DataFurnace[19] (Supporting Information, Figure S4). Therefore, a constant oxide density of 4.60 g·cm^{-3} was assumed. Irradiation at the highest fluence of 2×10^{16} cm^{-2} reduces the layer thickness by ~4, 5, and 10 nm for a krypton ion energy of 4, 10, and 35 keV, respectively (for detailed sputter rates see Supporting Information, Table S1).

Impedance measurements were performed as a function of frequency to investigate the thickness of the metallic layers. The impedance analyzer measures the complex impedance $\underline{Z}$ of the devices. The admittance is the inverse of the impedance, and can be defined as a conductor and a capacitor in parallel

$$\underline{Y} = 1/\underline{Z} = G + j\omega C \tag{1}$$

The loss angle tan δ is defined as

$$\tan\delta = \frac{\mathrm{Re}\{Z\}}{\mathrm{Im}\{Z\}} \tag{2}$$

Figure 3a plots the capacitance and the loss angle in dependence of frequency for a virgin device. The capacitance is frequency-dependent and decreases slightly for frequencies below 1 MHz. This behavior is modeled by a constant phase element:

$$\underline{Z_{\mathrm{CP}}} = \frac{1}{T\cdot(j\omega)^n}, \tag{3}$$

where n is the nonlinearity factor, and T is a factor. For an ideal capacitor counts $n = 1$, and T equals the capacitance C. For our devices the value n is $n = 0.9788$. In parallel to the constant phase element a resistor models the leakage current. For frequencies greater than 1 MHz the loss angle increases. At high frequencies the capacitor shorts the resistor, and a second resistor in series becomes dominant. This resistor models contact and wire resistance ($R = 14\ \Omega$). Nevertheless, this simple model is not sufficient for most of the irradiated devices. Here a peak in the loss angle arises (Figure 3b) that can be modeled by a second constant-phase element and a resistor. In this case the oxide layer consists of two regions with different conductance. Because the capacitance is inversely proportional to the thickness, comparing the factor T of the constant phase elements after ion irradiation with the reference device (d_{ref}, T_{ref}) gives the thickness of the remaining oxide layer:

$$d = d_{\mathrm{ref}}\cdot\frac{T_{\mathrm{ref}}}{T} \tag{4}$$

The sum of the corresponding extracted layer thicknesses gives the thickness of the insulating layer (Supporting Information, Figure S5). In contrast to the total thickness derived by the RBS analysis, the insulating oxide layer is thinner. The thickness difference can be attributed to a metallic NbO_x layer, which has a negligible capacitance.

In addition, from the oxide thickness and the corresponding resistor the small signal resistance R′ per nm is derived:

$$R' = \frac{R}{d} \tag{5}$$

Model. On the basis of the derived information a comprehensive model of the devices after ion irradiation is developed, and the results of the impedance data are displayed in Figure 1c. (All model parameters are depicted in Supporting Information, Tables S2–S4.) It includes the thickness reduction due to sputtering, the resulting NbO_x layer thickness, and the small signal resistivity of the insulating Nb_2O_5 layers.

The model of the 4 keV series is derived straightforwardly. For all ion fluences the maximum ion range ($R_{\mathrm{max}} \approx 10$ nm) is lower than the reduced oxide layer thickness. Hence, interface mixing is negligible and oxygen sputtering is the origin of the metallic layer. Therefore, the NbO_x layer is located at the top electrode, and it is reasonable that it is followed by a Nb_2O_5 layer with smaller resistance. The development of the layer structure shows four interesting aspects:

- Above an ion fluence of 7×10^{15} cm^{-2} the thickness of the NbO_x layer stays constant at about 5 nm, even when the overall thickness is reduced. This can be explained as follows: at low fluences preferential sputtering removes more oxygen than niobium. When the steady state is reached, oxygen and niobium are sputtered equally; thus, the layer thickness is further reduced, but the composition gradient remains unchanged.

dx.doi.org/10.1021/am5021149 | ACS Appl. Mater. Interfaces 2014, 6, 17474–17480

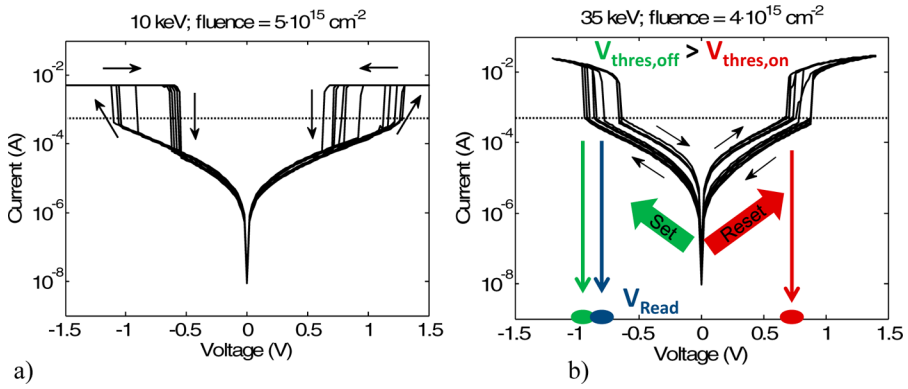

Figure 4. (a) Switching characteristic of a device limited by a current compliance (I_{cc} = 5 mA) and (b) of a device without current compliance. Limiting the current leads to pure threshold switching, whereas higher current adds a memory effect. The device of the left picture was irradiated with 10 keV Kr ions at a fluence of 5×10^{15} cm^{-2}, and the device of the right picture was irradiated with 35 keV Kr ions at an ion fluence of 4×10^{15} cm^{-2}. The arrows indicate the switching direction, and the dotted line indicates the threshold current I_{thres} where the abrupt increase in conductivity starts. Each picture shows six switching cycles.

- The thickness of the Nb_2O_5 layer with lower resistance due to defects and a slight stoichiometry unbalance also stays nearly constant at about 5 nm in the considered fluence range. The extension from surface equals the maximum ion range.
- The resistance per nm of the oxide layer near the bottom electrode decreases with increasing ion fluence. By thinning the oxide additional conduction mechanisms, for example, tunneling, have a higher probability. In addition, mobile defects caused by the ion irradiation accumulate near the bottom electrode.
- At the highest fluence the two layers affected by the krypton ions—the metallic NbO_x layer and the less conductive Nb_2O_5 layer—sum to a total thickness of ~13.8 nm.

The 10 keV irradiation was designed not to affect the bottom electrode. However, because of the not-negligible thickness reduction caused by surface sputtering, the ions are able to reach the bottom electrode above a certain ion fluence threshold. This threshold can be precisely determined from the electrical data. For low ion fluences of $<5 \times 10^{15}$ cm^{-2} the $I-V$ characteristic is strongly unbalanced, and the oxide thickness slightly decreases linearly with fluence. The metallic layer mainly forms at the top electrode due to preferential sputtering. The layer thickness is reduced by about 1 nm with increasing the fluence to 7×10^{15} cm^{-2}. Now, first krypton ions can reach the bottom electrode. This is indicated in the $I-V$ curve by an increase in the overall current for positive bias voltage, as shown in Figure 1b. Hence, interface mixing forms another metallic layer at the bottom electrode. An assumption regarding the thickness of the NbO_x layers is necessary, since from the electrical data one could not distinguish between NbO_x layers at bottom and top electrodes. We assumed the NbO_x layer at the top electrode stays constant at 7.5 nm according to the 4 keV situation, as the ion range remains constant, and thus the layer at the bottom electrode is ~1 nm.

For fluences of 9×10^{15} cm^{-2} or higher the $I-V$ characteristic becomes symmetric, and both interfaces to the electrodes are balanced. This is modeled by an increased NbO_x layer thickness at the bottom electrode but also by a change in conductance of the entire remaining oxide layers due to irradiation-induced defect formation.

For devices irradiated with 35 keV Kr ions the $I-V$ characteristic is reversed. Here, interface mixing at the bottom electrode is the dominant effect due to the high ion range. Nevertheless, in comparison to the 10 keV series for ion fluences below 7×10^{15} cm^{-2} the overall metallic layer thickness is smaller. Because interface mixing is expected to provide a thick metallic layer at the bottom electrode, the metallic layer at the surface caused by preferential sputtering must be thin (1 nm). In addition the resistivity of the insulating layer is lower compared to samples, which were irradiated with lower ion energies (see above). However, for ion fluences $\geq 9 \times 10^{15}$ cm^{-2} the thickness of the insulating layer decreases rapidly.

Switching Behavior. Finally, the switching behavior of the irradiated samples was investigated. It is well-known that resistive switching requires an initial electroforming step to build a conductive filament.[1,2] An important point for successful forming is the defect density of the oxide. On the one hand, devices with a thick and defect-free oxide need a high forming voltage. The voltage charges the capacitance and is discharged through the filament during forming. The resulting current overshoot increases the possibility of an irreversible hard breakdown.[20] In accordance with our model (compare Figure 1c) this phenomenon can be observed for devices irradiated with 4 keV krypton ions and fluences below 7×10^{15} cm^{-2}. After forming, the devices are in a low ohmic state and cannot be reset to a high resistance state anymore (Supporting Information, Figure S6a).

On the other hand, if the defect density is high, the leakage current is already at a high level in the virgin state, and therefore the forming voltage cannot be reached without exceeding the current compliance during the electroforming process. This was found for devices irradiated with 10 as well as 35 keV krypton ions and fluences above 1×10^{16} cm^{-2} (Supporting Information, Figure S6b).

Voltage polarity for successful forming depends on the location of the oxygen deficiencies and thus on the position of the metallic NbO_x layer (Supporting Information, Figure S7). Devices treated only at the surface with low-energy ions can be formed with positive bias at top electrode. Negative polarities must be applied for devices of the 35 keV series. For low ion fluences of the 10 keV krypton irradiation positive forming voltages are required because the NbO_x layer is located at the top electrode. However, above an ion fluence of 9×10^{15} cm^{-2}

the second metallic layer at the bottom electrode enables forming in both polarities. (All forming characteristics are summarized in Supporting Information, Table S5.)

All devices successfully formed show threshold switching[8] and thus show an abrupt increase in conductivity above a certain current threshold I_{thres}. In addition, the choice of the current compliance defines whether a memory effect adds to the device or not. By limiting the current to 5 mA the device is prevented from a further soft breakdown and exhibits pure threshold switching. Figure 4a shows the $I-V$ characteristic of a device that was irradiated with 10 keV krypton ions and an ion fluence of 5×10^{15} cm^{-2} with a threshold current of $I_{thres} = 0.5$ mA. Operating the device without current compliance adds a memory effect (Figure 4b). A reasonable resistance change between on and off states by a factor of up to 4 can be measured at a bias voltage of 0.25 V. Because of the fixed threshold current I_{thres} the start of the threshold effect depends on the resistance in the on and off states of the devices. That is, the threshold voltage in the on state $V_{thres,on}$ and in the off state $V_{thres,off}$ are clearly separated. This effect can be used for reading the devices by applying a read voltage in set direction, which is centered between $V_{thres,on}$ and $V_{thres,off}$. In the case of the off state the threshold voltage is not reached, and a current of $I_{off} = 0.3$ mA is detected. In contrast, if the device is switched on, threshold switching increases the current to $I_{on} = 10$ mA. Thus, the threshold effect amplifies the memory window by more than a magnitude.

As all devices that were successfully formed show threshold switching, the desired forming characteristic might be decisive for the choice of the optimum irradiation condition. For positive forming voltages the device should be irradiated with 4 keV and a high fluence of 2×10^{16} cm^{-2} to decrease the forming voltage. As an alternative approach lower fluences and reduced initial oxide thickness could be used. In that case no oxide layer thinning is performed, while the effect of preferential sputtering forms the NbO_x layer already at low fluences. For a gradient at the bottom electrode interface a high irradiation energy of 35 keV should be used with fluences of $4-5 \times 10^{15}$ cm^{-2} since the damage is already enough to achieve the desired decrease in forming voltage. If the devices should be formed in positive and negative directions, an energy of 10 keV and a fluence of 9×10^{15} cm^{-2} should be used.

CONCLUSIONS

Summarizing, metal−insulator−metal devices consisting of one insulating Nb_2O_5 layer were irradiated with krypton ions to form a metallic NbO_x sublayer to introduce threshold switching. Two effects were identified that induce this metallic NbO_x layer: preferential sputtering at the sample surface and interface mixing at the bottom electrode. These krypton-irradiated devices can be operated either as a pure threshold switch or as a combination of both threshold switch and memory element. The presented fabrication method enables cost-efficient device manufacturing, since ion irradiation could be structured easily using well-established lithography methods. Thus, the threshold switch can be formed in defined areas, for example, the intersection of top and bottom electrode in cross-bar arrays.

EXPERIMENTAL SECTION

Device Fabrication. Silicon wafers with 100 nm silicon dioxide grown by wet oxidation were used as substrate. A 4 nm titanium adhesion layer and a 20 nm thick platinum layer were sputtered as unstructured bottom electrode. Subsequently, a 20 nm thick layer of amorphous Nb_2O_5 was reactively sputtered from a metallic niobium target.[6] At this fabrication stage the ion beam irradiation took place (details see below). Finally, top electrodes were deposited by evaporating 40 nm platinum through a shadow mask with diameters ranging from 20 to 100 μm. 50 μm dots were used for electrical characterization, and 100 μm dots were used for impedance analysis.

Ion Irradiation. Three series of samples were irradiated with krypton ions at an ion energy of 4, 10, and 35 keV and fluences ranging from 4×10^{15} cm^{-2} to 2×10^{16} cm^{-2}, respectively. The ion flux was kept constant at 2.5×10^{12} cm^{-2} s^{-1}. The irradiation was done in normal direction at room temperature.

Raman. Raman shift was measured with a RenishawInVia microscope system using 514 nm excitation wavelength. Unfortunately, the devices described above are too thin for a reasonable signal. Therefore, special devices with 50 nm of oxide thickness were fabricated. To rank our results, three samples were studied comparatively: a reference device, a device sputtered at a lower oxygen-to-argon ratio flow (36.7% instead of 40%) resulting in a NbO_x layer and a Kr-irradiated device. Because the Nb_2O_5 layer is thicker the ion energy is adjusted to 40 keV. This corresponds to the case shown in the middle column of Figure 1a—most ions stop directly in front of the bottom electrode. The fluence of the irradiation was 1×10^{16} cm^{-2}.

RBS. Rutherford backscattering spectrometry using 2.5 MeV He ions and a backscattering angle of 170° was performed to determine compositional and thickness changes originating from the Kr irradiation. All samples were measured without top electrode and off-normal under a tilting angle of 75° to increase the depth resolution.

Electrical Measurements. Electrical characteristics and switching behavior were investigated using a Keithley 4200A semiconductor parameter analyzer. Thereby the analyzer applied a direct current voltage to the top electrode and grounded the bottom electrode. An Agilent impedance analyzer (4294A) measured the impedance in a frequency range from 40 Hz to 50 MHz. Open/Short/Load compensation was used for calibration. The fitting program LEVM was used for data analysis.[21,22]

ASSOCIATED CONTENT

Supporting Information

$I-V$ characteristic of an untreated device; full RBS spectra; atomic force microscope image of an untreated device and a device irradiated with krypton ions at 35 keV and 1×10^{16} cm^{-2}; remaining thickness of the complete Nb_2O_5/NbO_x stack as a function of ion fluence; sputter rate and sputter coefficient of amorphous Nb_2O_5 sputtered by krypton ions for 4, 10, and 35 keV irradiation energy; thickness of the insulating Nb_2O_5 layer as a function of the ion fluence; model parameter for the 4, 10, and 35 keV irradiation; forming characteristic. This material is available free of charge via the Internet at http://pubs.acs.org.

AUTHOR INFORMATION

Corresponding Authors

*E-mail: helge.wylezich@namlab.com. (H.W.)
*E-mail: stefan.slesazeck@namlab.com. (S.S.)

Author Contributions

The manuscript was written through contributions of all authors. All authors have given approval to the final version of the manuscript.

Notes

The authors declare no competing financial interest.

ACKNOWLEDGMENTS

This work has been financed by the Initiative and Networking Fund of German Helmholtz Association, Helmholtz Virtual

Institute VH-VI-422 MEMRIOX. We thank J. Gärtner and F. Nierobisch for the technical assistance. The ion irradiations were performed at the Ion Beam Center (IBC) of the Helmholtz−Zentrum Dresden Rossendorf and at the Friedrich Schiller University of Jena.

■ ABBREVIATIONS

MIS, metal insulator semiconductor
I−*V* characteristic, voltage−current characteristic
RBS, Rutherford backscattering spectrometry

■ REFERENCES

(1) Waser, R.; Dittmann, R.; Staikov, G.; Szot, K. Redox-Based Resistive Switching Memories—Nanoionic Mechanisms, Prospects, and Challenges. *Adv. Mater.* **2009**, *21*, 2632−2663.
(2) Sawa, A. Resistive Switching in Transition Metal Oxides. *Mater. Today* **2008**, *11*, 28−36.
(3) Yanagida, T.; Nagashima, K.; Oka, K.; Kanai, M.; Klamchuen, A.; Park, B. H.; Kawai, T. Scaling Effect on Unipolar and Bipolar Resistive Switching of Metal Oxides. *Sci. Rep.* **2013**, *3*, 1657.
(4) Flocke, A.; Noll, T. G. Fundamental Analysis of Resistive Nano-Crossbars for the Use in Hybrid Nano/CMOS-Memory. *Proc. ESSCIRC* Munich, **2007**, *33*, 328−331.
(5) Shenoy, R. *Challenges for Selector Devices;* Tutorial at International Memory Workshop (IMW): Monterey, CA, May 2013.
(6) Mähne, H.; Berger, L.; Martin, D.; Klemm, V.; Slesazeck, S.; Jakschik, S.; Rafaja, D.; Mikolajick, T. Filamentary Resistive Switching in Amorphous and Polycrystalline Nb2O5 Thin Films. *Solid-State Electron.* **2012**, *72*, 73−77.
(7) Pickett, M. D.; Williams, R. S. Sub-100 fJ and Sub-Nanosecond Thermally Driven Threshold Switching in Niobium Oxide Crosspoint Nanodevices. *Nanotechnology* **2012**, *23*, 215202.
(8) Mähne, H.; Wylezich, H.; Slesazeck, S.; Mikolajick, T.; Vesely, J.; Klemm, V.; Rafaja, D. Room Temperature Fabricated NbOx/Nb2O5Memory Switching Device with Threshold Switching Effect. *Proc. IMW,* Monterey, CA, **2013**, *5*, 174−177.
(9) Bae, J.; Hwang, I.; Jeong, Y.; Kang, S. O.; Hong, S.; Son, J.; Choi, J.; Kim, J.; Park, J.; Seong, M. J.; Jia, Q.; Park, B. H. Coexistence of Bi-Stable Memory and Mono-Stable Threshold Resistance Switching Phenomena in Amorphous NbOx Films. *Appl. Phys. Lett.* **2012**, *100*, 062902.
(10) Cha, E.; Woo, J.; Lee, D.; Lee, S.; Song, J.; Koo, Y.; Lee, J. H.; Park, C. G.; Yang, M. Y.; Kamiya, K.; Shiraishi, K.; Magyari-Köpe, B.; Nishi, Y.; Hwang, H. Nanoscale (~10nm) 3D Vertical ReRAM and NbO2 Threshold Selector with TiN Electrode. *Proc. IEDM,* Washington, DC, **2013**, *13*, 268−271.
(11) Liu, X.; Sadaf, S. M.; Son, M.; Park, J.; Shin, J.; Lee, W.; Seo, K.; Lee, D.; Hwang, H. Co-Occurrence of Threshold Switching and Memory Switching in Cells for Crosspoint Memory Applications. *IEEE Electron Device Lett.* **2012**, *33*, 236−238.
(12) Murti, D. K.; Kellya, R. Preferential Oxygen Sputtering from Nb2O5. *Thin Solid Films* **1976**, *33*, 149−163.
(13) Choudhury, T.; Saied, S. O.; Sullivan, J. L.; Abbot, A. M. Reduction of Oxides of Iron, Cobalt, Titanium and Niobium by Low-Energy Ion Bombardment. *J. Phys. D: Appl. Phys.* **1989**, *22*, 1185.
(14) Ziegler, J.; Biersack, J.; Littmark, U. *The Stopping and Range of Ions in Matter;* Pergamon: New York, 1985.
(15) Nowak, I.; Ziolek, M. Niobium Compounds: Preparation, Characterization, and Application in Heterogeneous Catalysis. *Chem. Rev.* **1999**, *99*, 3603−3624.
(16) Jehng, J. M.; Wachs, I. E. Structural Chemistry and Raman Spectra of Niobium Oxides. *Chem. Mater.* **1991**, *3*, 100−107.
(17) Michaelson, H. B. The Work Function of the Elements and its Periodicity. *J. Appl. Phys.* **1977**, *48*, 4729−4733.
(18) Hickmott, T. W. Electroluminescence and Conduction in Nb−Nb2O5−Au Diodes. *J. Appl. Phys.* **1966**, *37*, 4380−4388.
(19) Jeynes, C.; Barradas, N. P.; Marriott, P. K.; Boudreault, G.; Jenkin, M.; Wendler, E.; Webb, R. P. Elemental Thin Film Depth Profiles by Ion Beam Analysis Using Simulated Annealing—A New Tool. *J. Phys. D: Appl. Phys.* **2003**, *36*, 97−126.
(20) Gilmer, D. C.; Bersuker, G.; Park, H. Y.; Park, C.; Butcher, B.; Wang, W.; Kirsch, P. D.; Jammy, R. Effects of RRAM Stack Configuration on Forming Voltage and Current Overshoot. *Proc. IMW,* Monterey, CA, **2011**, *3*, 1−4.
(21) Macdonald, J. R. *LEVM/LEVMW Manual,* Version 8.10; J. R. Macdonald at University of North Carolina: Chapel Hill, NC, 2010.
(22) Macdonald, J. R. *Impedance Spectroscopy;* Wiley: New York, 1987.